RNA (1998), *4*:542–550. Cambridge University Press. Printed in the USA.

Matching the crystallographic structure of ribosomal protein S7 to a three-dimensional model of the 16S ribosomal RNA

ISAO TANAKA,[1] ATSUSHI NAKAGAWA,[1] HARUMI HOSAKA,[1] SOICHI WAKATSUKI,[2] FLORIAN MUELLER,[3] and RICHARD BRIMACOMBE[3]

[1]Graduate School of Science, Hokkaido University, Sapporo 060, Japan
[2]European Synchrotron Radiation Facility, Polygone Scientifique, Avenue des Martyrs, 38043 Grenoble, France
[3]Max-Planck-Institut für Molekulare Genetik, Ihnestrasse 73, 14195 Berlin, Germany

ABSTRACT

Two recently published but independently derived structures, namely the X-ray crystallographic structure of ribosomal protein S7 and the "binding pocket" for this protein in a three-dimensional model of the 16S rRNA, have been correlated with one another. The known rRNA–protein interactions for S7 include a minimum binding site, a number of footprint sites, and two RNA–protein crosslink sites on the 16S rRNA, all of which form a compact group in the published 16S rRNA model (despite the fact that these interactions were not used as primary modeling contraints in building that model). The amino acids in protein S7 that are involved in the two crosslinks to 16S rRNA have also been determined in previous studies, and here we have used these sites to orient the crystallographic structure of S7 relative to its rRNA binding pocket. Some minor alterations were made to the rRNA model to improve the fit. In the resulting structure, the principal positively charged surface of the protein is in contact with the 16S rRNA, and all of the RNA–protein interaction data are satisfied. The quality of the fit gives added confidence as to the validity of the 16S rRNA model. Protein S7 is furthermore known to be crosslinked both to P site-bound tRNA and to mRNA at positions upstream of the P site codon; the matched S7-16S rRNA structure makes a prediction as to the location of this crosslink site within the protein molecule.

Keywords: cryo-electron microscopy; molecular modeling; ribosomal RNA (rRNA); RNA–protein interaction; X-ray crystallography

INTRODUCTION

Three independent approaches to the study of the bacterial ribosome are rapidly converging to give a new insight into the structure and function of this particle. The three approaches are: (1) derivation of computerized three-dimensional (3D) reconstructions of the ribosome based on cryo-electron microscopy; (2) development of 3D models for the ribosomal RNA based on biochemical evidence and subsequently fitted to the electron microscopic (EM) structures; and (3) determination of structures of the individual ribosomal proteins at atomic resolution by X-ray crystallography and NMR.

Recent advances that have been made in the cryo-electron microscopy of 70S ribosomes (Frank et al., 1995; Stark et al., 1995, 1997a, 1997b; Agrawal et al., 1996) have resulted in computerized reconstructions of the particles that have now reached a resolution of better than 20 Å. In particular, tRNA molecules at the ribosomal A, P, or E sites can be directly visualized in these reconstructions (Agrawal et al., 1996; Stark et al., 1997a, 1997b), so that the decoding site on the small (30S) subunit and the peptidyl transferase center on the large (50S) subunit can be located with considerable precision. For the 30S subunit, there is an enormous amount of biochemical evidence that is relevant to the 3D folding of the *Escherichia coli* 16S rRNA (see, e.g., Brimacombe, 1995, for review), and this evidence includes several data sets relating specific sites on the 16S molecule to corresponding sites on tRNA or mRNA in the decoding region. By combining this information with the fine structure that is visible in the EM reconstructions, it has been possible to adapt our previous model for the 3D folding of the 16S rRNA so that it fits the 30S moiety of the 70S EM structure (Mueller & Brimacombe 1997a). This model-building strategy contrasts with older studies (e.g., Brimacombe et al., 1988; Stern et al., 1988), where the known 3D arrangement

Reprint requests to: Richard Brimacombe, Max-Planck-Institut für Molekulare Genetik, Ihnestrasse 73, 14195 Berlin, Germany.

of the 30S ribosomal proteins was combined with RNA–protein interaction data in order to model the 16S rRNA. The protein arrangement is based on immune electron microscopic (Lake, 1982; Stöffler & Stöffler-Meilicke, 1984) and neutron scattering (Capel et al., 1988) investigations, whereas the RNA–protein interaction data were derived from extensive RNA–protein footprinting (Stern et al., 1988) and crosslinking (Brimacombe, 1991) experiments. In the newer model (Mueller & Brimacombe, 1997a), these RNA–protein interaction data [as well as the newer results of Powers & Noller (1995)] were not taken into account as primary constraints in the model-building process, but were nevertheless subsequently used to correlate the EM-fitted 16S rRNA structure with the 3D arrangement of the proteins (Mueller & Brimacombe, 1997b).

Parallel to these developments, a number of X-ray crystallographic or NMR structures have been determined for the individual ribosomal proteins. In the case of the 30S subunit, these include proteins S5 (Ramakrishnan & White, 1992), S6 (Lindahl et al., 1994), S7 (Hosaka et al., 1997; Wimberly et al., 1997), S8 (Davies et al., 1996), S15 (Berglund et al., 1997), and S17 (Golden et al., 1993). The most recent structure—that of protein S7—has been determined independently by two research groups (Hosaka et al., 1997; Wimberly et al., 1997); the two structures are essentially identical. S7 is of particular interest because this protein is known to be in close contact both with the anticodon loop of P site-bound tRNA (Wower et al., 1993; Döring et al., 1994) and with the mRNA just upstream of the decoding region (Stade et al., 1989). Furthermore, the protein contains two sites of crosslinking to the 16S rRNA that have been determined at the amino acid/nucleotide level (Möller et al., 1978; Urlaub et al., 1997), and its minimum binding site on the 16S rRNA has also been established (Dragon & Brakier-Gingras, 1993; Dragon et al., 1994). The rRNA regions concerned, as well as the corresponding footprint sites for S7 on the 16S rRNA (Stern et al., 1988; Powers & Noller, 1995), are concentrated into a compact group in the new model (Mueller & Brimacombe, 1997b). Because the X-ray structure of S7 (Hosaka et al., 1997) and the 3D model for the 16S rRNA (Mueller & Brimacombe, 1997a) were derived entirely independently of one another, an obvious challenge now is to ask how well the two structures fit together; this offers a searching test of the validity and accuracy of the 16S rRNA model in the S7 contact area.

In this paper, we show that the X-ray crystallographic structure of protein S7 can indeed be matched to the 16S rRNA model in a manner that satisfies all the biochemical data just mentioned, and that, at the same time, shows a plausible correspondence with the putative RNA binding surfaces of the protein (Hosaka et al., 1997). One helix of the 16S rRNA was rotated slightly in the model so as to generate an even better fit to the RNA–protein footprinting data of Powers and Noller (1995), and the configurations of two single strands were modified to give a precise fit to the crosslink sites of Urlaub et al. (1997). The final arrangement makes the prediction that the contact between protein S7 and the anticodon loop of P site tRNA or the upstream region of the mRNA lies either within the β-sheet region of the protein (between residues ca. 75–90), or in the region of the C-terminus of the sixth α-helix (residues ca. 145–155) (Hosaka et al., 1997).

RESULTS AND DISCUSSION

RNA–protein interaction data between the 16S rRNA and protein S7

The sites on *E. coli* 16S rRNA that have been implicated in interactions with S7 are summarized in Figure 1. These include sites of hydroxyl radical footprinting by Fe(II)-EDTA from Powers and Noller (1995), the older base-specific footprint sites from the same laboratory (Stern et al., 1988), and sites of crosslinking induced either by direct UV-irradiation (Möller et al., 1978) or by treatment with bifunctional reagents (Brimacombe, 1991). The minimal binding site for S7 deduced by Dragon and Brakier-Gingras (1993) is also included. It can be seen that all of this information is located within helices 28–30 and 41–43 of the 16S rRNA [helix numbering as in Mueller & Brimacombe (1997a)], which forms part of the 3′-domain of the 16S molecule. The 3′-domain comprises the "head" region of the 30S ribosomal subunit (see, e.g., Stern et al., 1988; Mueller & Brimacombe, 1997a).

The structure of protein S7 from *Bacillus stearothermophilus* (Hosaka et al., 1997) is shown in Figure 2. The figure indicates the locations of the sites of crosslinking to 16S rRNA (Urlaub et al., 1997) within the protein "backbone;" these sites correspond to those shown in Figure 1. Figure 2 also illustrates the areas of positively charged surface expected to be in contact with the rRNA. Protein S7 from *B. stearothermophilus* (Kimura, 1991) has a high degree of homology (58%) to its counterpart from *E. coli* (Reinbolt et al., 1978), and the RNA–protein crosslink sites on the protein have been determined for both organisms (Urlaub et al., 1995, 1997). In the earlier of these two publications, using *B. stearothermophilus* (Urlaub et al., 1995), only the crosslinking sites on the protein were analyzed, and their correspondence with the crosslinked partners on the rRNA was inferred by comparison with previous data (Brimacombe, 1991). In the more recent publication (Urlaub et al., 1997), the sites of crosslinking on both the RNA and the protein moieties were determined diirectly by mass spectrometry of crosslinked oligonucleotide–peptide complexes, in the *E. coli* system. These data confirmed the previously identified crosslink, directly induced by UV-irradiation, between U-1240

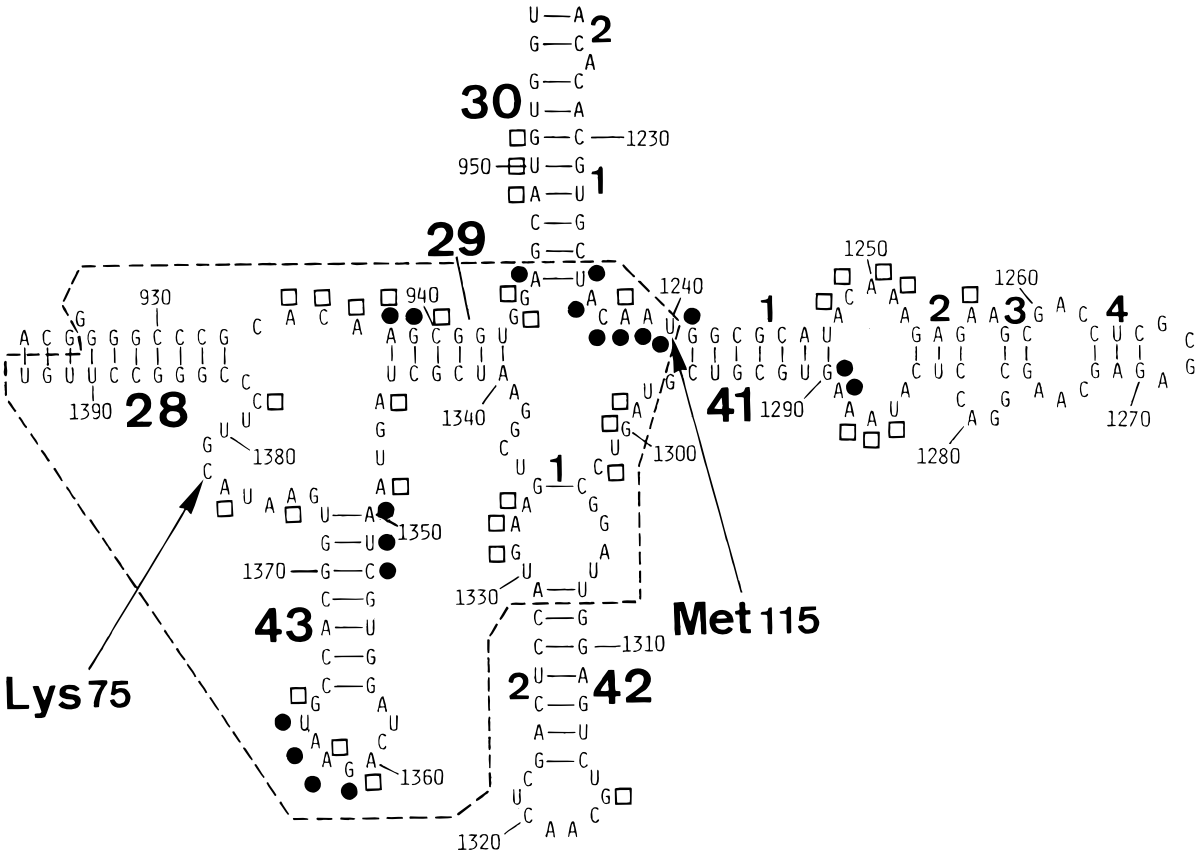

FIGURE 1. Part of the secondary structure of the *E. coli* 16S rRNA, showing sites implicated in interaction with protein S7. Helices are numbered as in Mueller and Brimacombe (1997a), including the subdivisions of the helices (e.g., helix 41 is divided into four parts, numbered 1–4, which in the following computer-generated figures are denoted by h41d1–h41d4). Fe(II)-EDTA footprint sites for S7 (Powers & Noller, 1995) are marked by solid circles, base-specific footprint sites (Stern et al., 1988) by open squares. Positions of crosslinking to Met-115 and Lys- or Arg-75 [see text and Urlaub et al. (1997)] are indicated by arrows. The minimum binding site for S7 on the rRNA (Dragon & Brakier-Gingras, 1993) is enclosed by the dashed line.

of the 16S rRNA (Zwieb & Brimacombe, 1979) and Met-115 [using *B. stearothermophilus* numbering, cf. Hosaka et al. (1997)] in protein S7 (Möller et al., 1978). The second crosslink (Urlaub et al., 1997), which was induced by treatment with the bifunctional reagent 2-iminothiolane (cf. Brimacombe, 1991), was localized to C-1378 of the 16S rRNA and Lys-75 in the *E. coli* S7 sequence; the latter residue is arginine in *B. stearothermophilus* (Hosaka et al., 1997).

Matching the S7 structure to the 16S rRNA model

In the recently published model for the 3D folding of the *E. coli* 16S rRNA (Mueller & Brimacombe, 1997a), the 16S molecule was fitted to the 30S moiety of the EM reconstruction at 19 Å resolution of 70S ribosomes carrying tRNA molecules at the A and P sites (Stark et al., 1997a). The neutron scattering map for the mass centers of the 30S ribosomal proteins (Capel et al., 1988) was fitted to the same EM reconstruction. In the resulting structure, the RNA–protein interaction data for protein S7 are clustered into a compact group within the head region of the 30S subunit, closely surrounding the neutron position for the protein (Mueller & Brimacombe, 1997b).

The crystallographic structure for protein S7 (Hosaka et al., 1997) was accordingly combined with the 16S rRNA model (Mueller & Brimacombe, 1997a, 1997b), using the program ERNA-3D (Mueller & Brimacombe, 1997a), and the resulting complex is illustrated in Figures 3, 4, and 5. It must be emphasized that these figures show the "raw" fit of the protein to the rRNA model, before any refinements were performed. Figure 3A shows a semi-transparent silhouette (without 16S rRNA) of the 30S moiety of the EM reconstruction (Stark et al., 1997a), with the neutron positions of the proteins superimposed as in Mueller and Brimacombe (1997b). Protein S7 is highlighted in red, and the crystal structure of S7 (Hosaka et al., 1997) in its fitted position is shown as the green "backbone" model. It should be noted that the dimensions of the protein

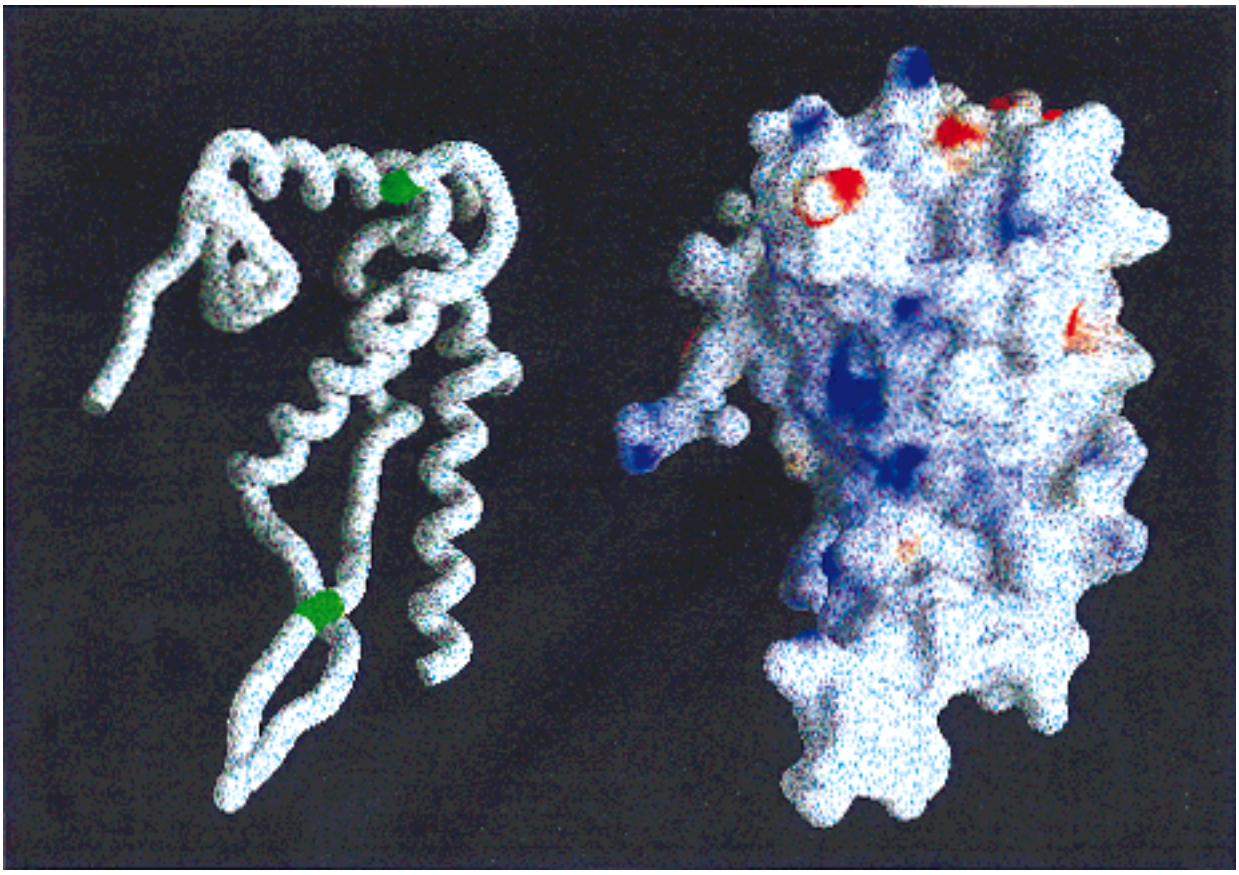

FIGURE 2. Structure of protein S7 (adapted from Hosaka et al., 1997), showing (left) the backbone of the protein and (right) the electrostatic surface potential. The orientation of the structure is the same in both cases, with the N-terminal region of the protein on the upper left and the C-terminal α-helix on the lower right. The two crosslinks to 16S rRNA are highlighted in green on the protein backbone; Met-115 is on the upper right, and Arg-75 (which is lysine in the *E. coli* protein sequence; see text) is lower center. The electrostatic surface potential is displayed as a color gradient from red (electronegative) to blue (electropositive), generated using the program GRASP (Nicholls et al., 1991), as in Hosaka et al. (1997).

spheres representing the neutron map are reduced to about two-thirds of their size as depicted by Capel et al. (1988), for better visibility. The position of the S7 crystal structure in Figure 3A corresponds well with its location in the neutron map, with the lower apex of the protein lying close to the P site tRNA (Mueller et al., 1997; Stark et al., 1997a) and the immediate upstream region of the mRNA, as expected from the crosslinking data (Stade et al., 1989; Wower et al., 1993; Döring et al., 1994) quoted in the Introduction. This can be seen more clearly in the close-up view of Figure 3B, where the lower apex of S7 lies close to the hole in the 30S subunit head region through which the incoming mRNA chain passes (Mueller et al., 1997).

The correspondence with the biochemical data of Figure 1 is illustrated in Figures 4 and 5. Figure 4A shows the elements of 16S rRNA that comprise the minimum binding site for S7 (Dragon & Brakier-Gingras, 1993; Dragon et al., 1994), together with the fitted protein structure, whereas Figure 4B gives the locations of the base-specific (Stern et al., 1988) and Fe(II)-EDTA (Powers & Noller, 1995) footprint sites for S7, highlighted as ball-and-stick nucleotides (cf. Mueller & Brimacombe, 1997b) within the appropriate elements of the 16S molecule. As pointed out by Powers and Noller (1995), the Fe(II)-EDTA footprint data are more concise than their base-specific counterparts, and the Fe(II)-EDTA sites are shown alone in the stereo view of Figure 5A. These sites clearly fit well to the protein structure, with the exception of the sites in helix 43 (on the right in Fig. 5A), which are displaced slightly to the right of the protein molecule. Figure 5B shows the positions of the two crosslink sites between S7 and the 16S rRNA [Fig. 1 and Urlaub et al. (1997)], which also fit reasonably well to the protein structure. The crosslink sites on the 16S rRNA both lie in single-stranded regions (nt 1236–1240, and 1373–1383, respectively), and these single strands do not have rigidly defined configurations in the 16S rRNA model (Mueller & Brimacombe, 1997a). The crosslink site at nt 1378, which lies in the middle of the long single strand between nt 1373 and 1383, is obviously particularly flexible. Some adjust-

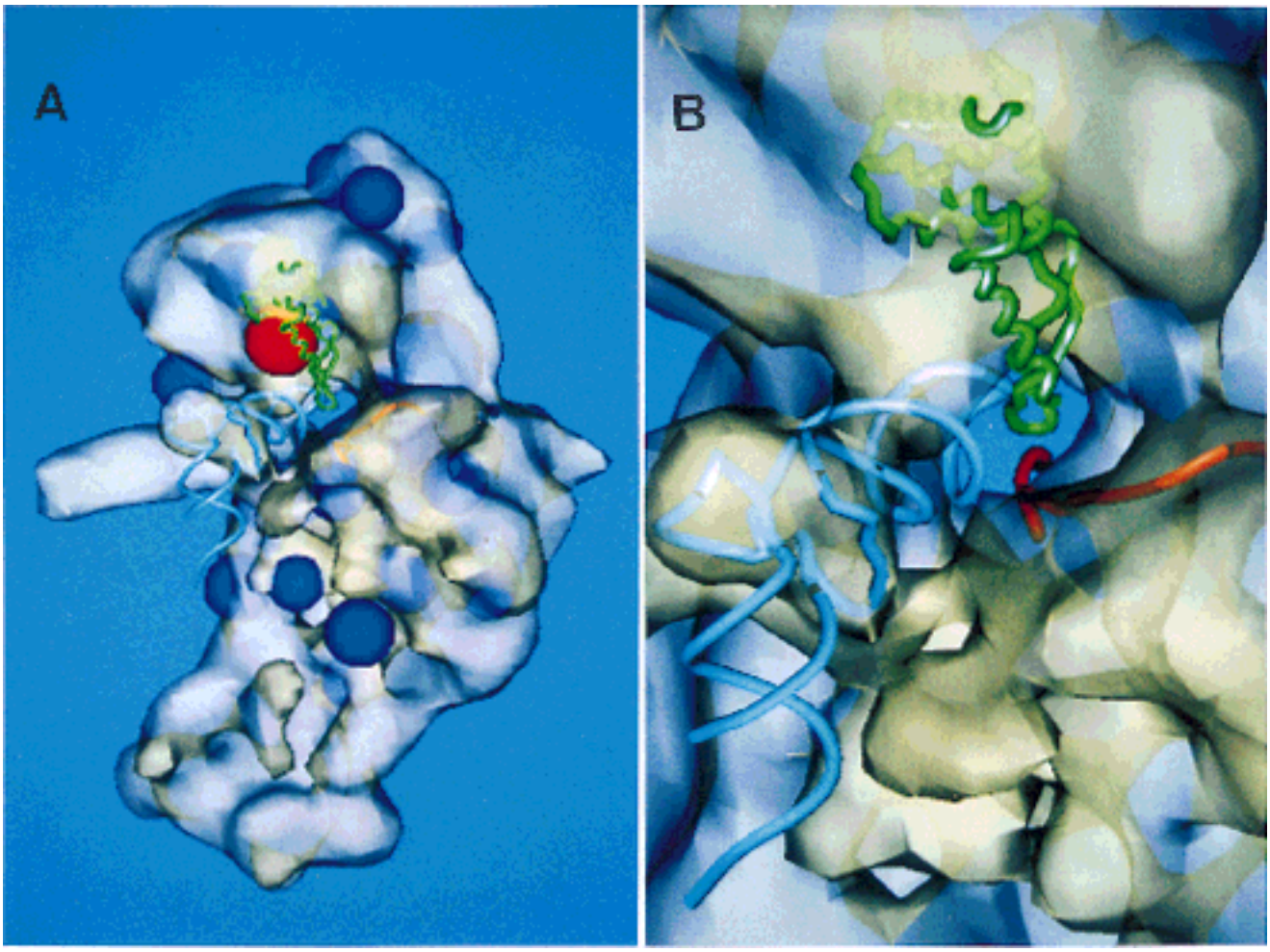

FIGURE 3. Location of protein S7 in the *E. coli* 30S subunit. **A:** Semi-transparent silhouette of the 30S subunit, with the neutron map of the 30S ribosomal proteins (Capel et al., 1988) fitted to the structure as in Mueller and Brimacombe (1997b); the proteins are represented by the blue spheres, with the exception of S7, which is red. (A number of the blue protein spheres are "buried" within the 30S silhouette.) The backbone of the crystal structure of S7 (Hosaka et al., 1997) is superimposed in green (cf. Fig. 2). Backbone structures of the P site tRNA and a segment of mRNA in the decoding region (positioned as in Mueller et al., 1997) are shown in blue and red, respectively. **B:** Close-up of the backbone of the crystal structure of protein S7, together with P site tRNA and mRNA within the 30S subunit, color-coded and oriented as in A.

ments of the model in these areas are thus possible, without disturbing the arrangement of the 16S rRNA helices.

Refinement of the 16S model to improve the match to protein S7

Two minor refinements were made to the 16S model, so as to improve the fit to the S7 crystal structure (Hosaka et al., 1997) as shown in Figures 4 and 5. First, helix 43 was rotated slightly about its own helical axis, so as to bring the Fe(II)-EDTA footprint sites in this helix (cf. Figs. 1, 5A) closer to the S7 molecule. Because helix 43 occupies a relatively "isolated" position in the 16S model (Mueller & Brimacombe, 1997a) and is connected to the neighboring helices (helices 28 and 29, Fig. 1) by flexible single strands, this could be accomplished without influencing the rest of the 16S structure or violating the EM contour. Secondly, the single strands containing the crosslink sites at nt 1240 and 1378 were manipulated, using the chain-pulling algorithm of ERNA-3D (Mueller & Brimacombe, 1997a), so as to bring the crosslink sites into closer contact with their counterparts in the S7 molecule, at Met-115 and Arg- or Lys-75, respectively. In the case of the site at nt 1378, this movement had the concomitant effect of bringing the crosslinked nucleotide closer to the anticodon loops of the tRNA molecules in the model (Mueller et al., 1997, and cf. Fig. 3B); nt 1378 is a target of crosslinking from position 32 of an A or E site-bound tRNA molecule (Döring et al., 1994).

The result of these improvements is illustrated in Figure 6, which is a view of the refined fit, showing the Fe(II)-EDTA footprint sites and the RNA–protein crosslink sites as in Figure 5A and B. The P site tRNA molecule and a segment of mRNA are also included in the

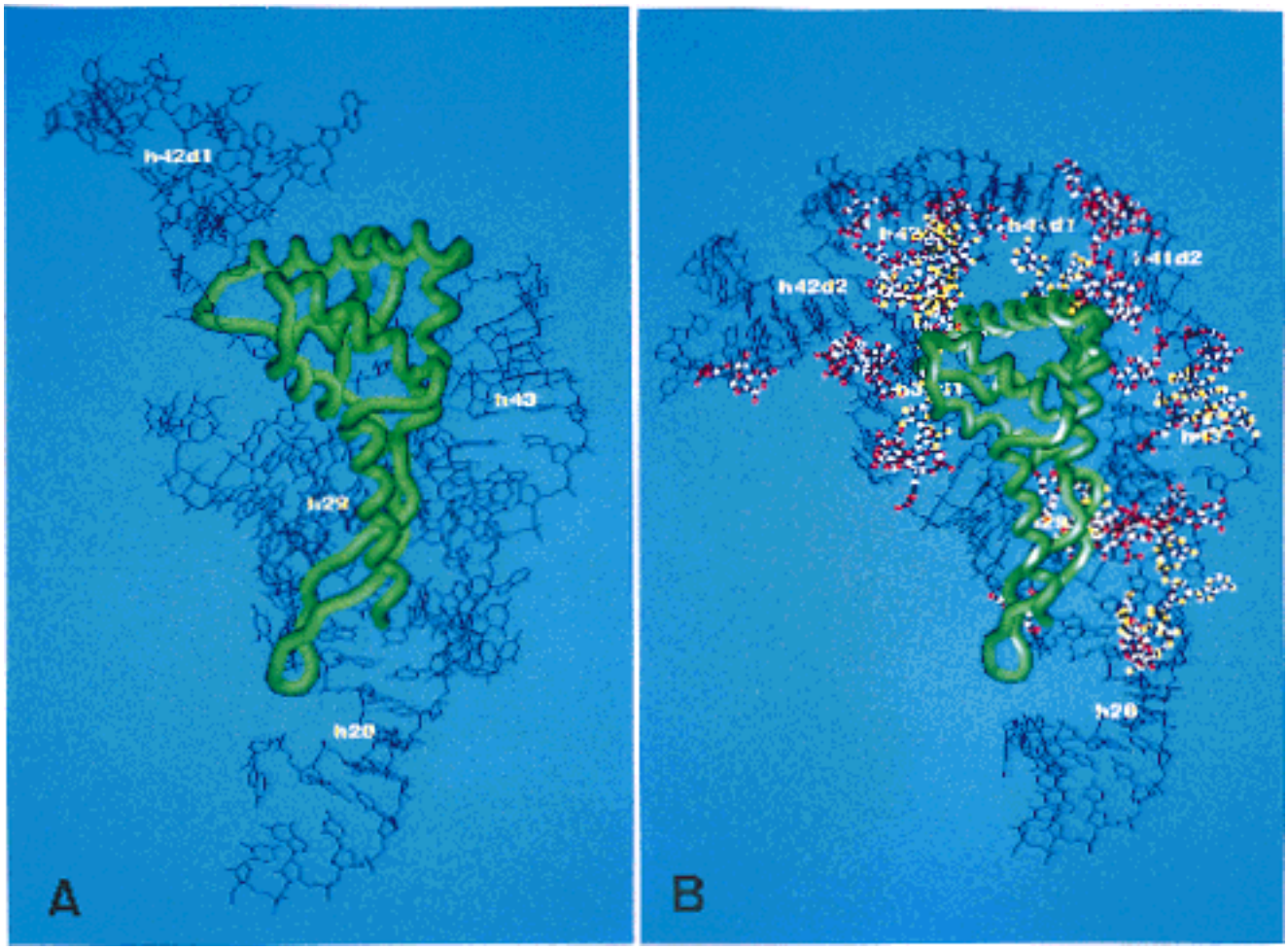

FIGURE 4. Protein S7 incorporated into the 16S rRNA model. **A:** Backbone of protein S7 (green), together with the elements of the 16S rRNA model (Mueller & Brimacombe, 1997a) comprising the minimum binding site for S7 (Dragon & Brakier-Gingras, 1993). The double-helical regions of the latter (helices 28, 29, 42-1, and 43) are numbered as in Figure 1. **B:** S7 backbone (green) together with elements of the 16S rRNA model (helices 28, 29, 30–1, 41–1, 41-2, 42-1, 42-2, and 43) containing footprint sites for S7 (cf. Mueller & Brimacombe, 1997b). Base-specific footprint sites (Stern et al., 1988) are highlighted as red ball-and-stick nucleotides, Fe(II)-EDTA footprint sites (Powers & Noller, 1995) as yellow ball-and-stick nucleotides. The orientation of the structure is approximately the same as that of Figure 3.

figure (cf. Mueller et al., 1997). By comparison with Figure 2, in which protein S7 is rotated about the vertical axis in relation to its orientation in Figure 6, it can be seen that the principal positively charged surface of the protein is mainly in contact with helix 29 (Fig. 6, center; cf. Fig. 5). This protein region comprises the two β-strands and the fourth α-helix (Hosaka et al., 1997), which also contact helix 43 (Fig. 6, right). It has been suggested (Wimberly et al., 1997) that the hairpin feature formed by the two β-strands could bind to the groove of double-stranded RNA, by virtue of its homology to the HU family of DNA-binding proteins (also observed by Hosaka et al., 1997). At the same time, however, Wimberly et al. (1997) noted that the hairpin is likely to be highly flexible in solution and to change its orientation upon binding to rRNA. Given this potential flexibility, it is not possible at the current level of resolution to judge how far such detailed predictions hold. The second α-helix of the protein is in contact with the rRNA helices 41-1 and 42-1 (cf. Fig. 1) in the upper part of Figure 6. The α-helices 1, 3, and 5 (Hosaka et al., 1997), on the other hand, are located on the outward-facing side of the protein. The crosslink sites in the revised model (Fig. 6) are now in close contact with their counterparts on the protein (cf. Fig. 5B), but it should be noted that—as emphasized in Mueller and Brimacombe (1997a, 1997b)—the single-stranded regions of the 16S molecule cannot be modeled accurately at the current level of resolution, and possible van der Waals conflicts with these single-stranded regions have not so far been considered. Nevertheless, there is a close correspondence between the structure of Figure 6 and the S7-16S rRNA minimum binding site described by Dragon and Brakier-Gingras (1993). Because S7 is known to be one of the two proteins responsible for initiating assembly of the 30S subunit

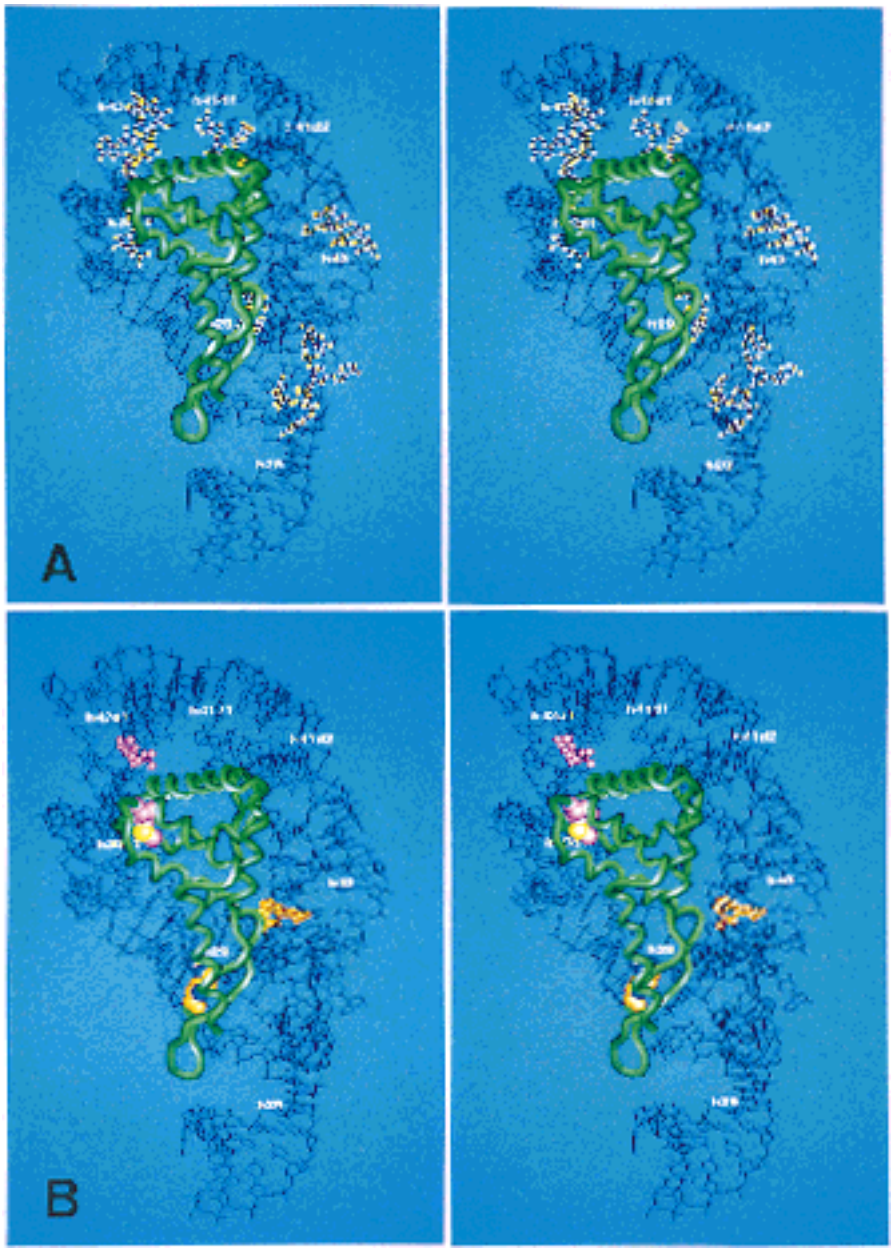

FIGURE 5. Stereo views of the Fe(II)-EDTA footprint sites and crosslink sites. **A:** Backbone of S7 (green) together with 16S rRNA helices as in Figure 4B. The Fe(II)-EDTA footprint sites (Powers & Noller, 1995) are also highlighted as in Figure 4B. **B:** Same rRNA helices together with the S7 backbone, showing the RNA–protein crosslink sites (Urlaub et al., 1997). The crosslink between Met-115 and U-1240 is highlighted in purple (with the sulfur atom of the methionine in yellow), and the crosslink between Lys-75 (arginine in the crystal structure; see text) and C-1378 is highlighted in orange (with the nitrogen atoms of the arginine in dark blue).

(Nowotny & Nierhaus, 1988), it seems likely that the correct folding of this rRNA region (Fig. 6) is crucial for the subsequent folding of the rest of the 3′ domain of the 16S rRNA.

The loop end of helix 43 points downward in the 16S rRNA model (in the orientation shown in Fig. 6), so as to accommodate the crosslink between nt 1360 in this loop end and the upstream region of mRNA (Rinke-Appel et al., 1994; Mueller et al., 1997). The loop end of helix 43 (lower right in Fig. 6) is also in close contact with S7, and it can be seen that the fitted structure predicts a contact between the immediate upstream region of the mRNA [or the anticodon loop of the tRNA (cf. Wower et al., 1993; Döring et al., 1994)] and the lower apex of the protein, either within the β-sheet region (amino acids ca. 75–90) or at the extreme C terminus (from amino acid ca. 145 within the terminal α-helix to the C terminus itself at position 155). Here it should be noted that the last eight amino acids are disordered and thus not included in the X-ray structure (Hosaka et al., 1997); this C-terminal sequence, RAFAHYRW, contains several positively charged and aromatic residues, which are good potential candidates for the interaction with mRNA. An experimental analysis of the site of crosslinking within the *E. coli* S7 protein from the upstream region of the mRNA (cf. Stade et al., 1989) is currently in progress (cf. Urlaub et al., 1997) to test this prediction.

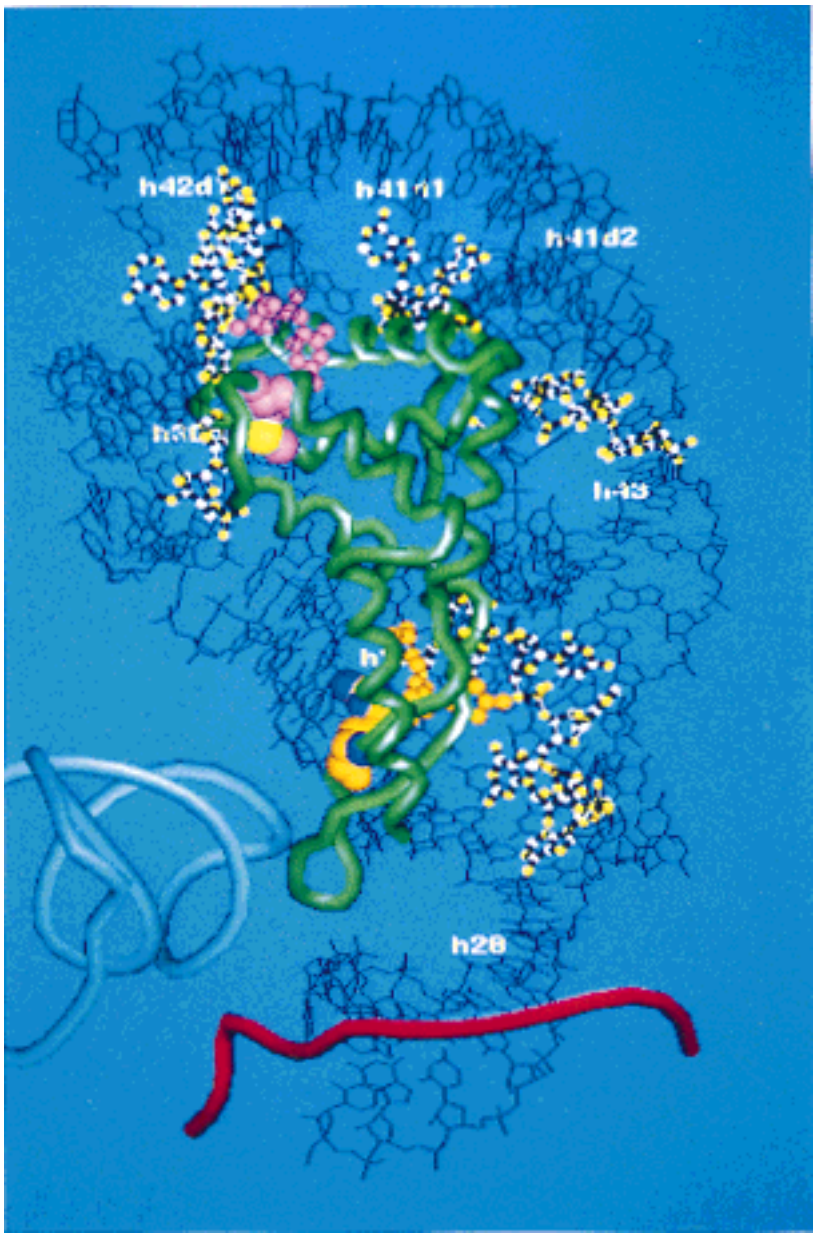

FIGURE 6. View of the S7-16S rRNA fit, after performing the minor refinements described in the text. The Fe(II)-EDTA footprint sites and crosslink sites are highlighted as in Figure 5A and B, respectively. The anticodon loop of P site tRNA and a segment of mRNA are included, colored light blue and red, respectively, as in Figure 3B.

CONCLUSIONS

Although the determination of the structure of a complete ribosome at atomic resolution still remains a long-term goal, atomic structures of individual ribosomal components or functional ligands are appearing in the literature with increasing frequency. The advent of the cryo-electron microscopic reconstructions at a resolution of 20 Å or better (Stark et al., 1997a, 1997b) now offers a means for locating these individual structures within the context of the whole ribosome. Some of the structures, notably the Ef-Tu/tRNA complex (Nissen et al., 1995) or the tRNA molecules themselves, can be fitted to corresponding regions of density that are directly identifiable in the appropriate EM reconstructions (Stark et al., 1997a, 1997b). In the case of the ribosomal proteins (where, as noted in the Introduction, six structures from the 30S subunit have already been solved), such a direct visualization is not possible, but the atomic structures of the proteins can nonetheless be matched to their binding pockets on the 16S rRNA model (Mueller & Brimacombe, 1997a, 1997b) via the RNA–protein interaction data, as we have shown here for protein S7 (Hosaka et al., 1997). The success of the fit between these two independently derived structures increases our confidence in the validity of the 16S rRNA model in those regions comprising the protein binding pocket, and begins as well to provide a detailed picture of the interaction of protein S7 with tRNA and mRNA at the decoding center of the ribosome.

METHODS

The molecular modeling procedures used and the program ERNA-3D have been described elsewhere (Hosaka et al., 1997; Mueller & Brimacombe, 1997a). Because the 16S rRNA model has not been subjected to energy minimization, the coordinates of the structure have not been deposited in the Brookhaven Protein Data Bank. The coordinates will, however, be provided on request from the Berlin laboratory (R.B. or F.M.).

Received December 19, 1997; returned for revision Febrary 10, 1998; revised manuscript received February 23, 1998

REFERENCES

Agrawal RK, Penczek P, Grassucci RA, Li H, Leith A, Nierhaus KH, Frank J. 1996. Direct visualization of A-, P-, and E-site transfer RNAs in the *E. coli* ribosome. *Science 271*:1000–1002.

Berglund H, Rak A, Serganov A, Garber M, Härd T. 1997. Solution structure of the ribosomal RNA binding protein S15 from *T. thermophilus. Nature Struct Biol 4*:20–23.

Brimacombe R. 1991. RNA–protein interactions in the *E. coli* ribosome. *Biochimie 73*:927–936.

Brimacombe R. 1995. The structure of ribosomal RNA: A three-dimensional jigsaw puzzle. *Eur J Biochem 230*:365–383.

Brimacombe R, Atmadja J, Stiege W, Schüler D. 1988. A detailed model of the three-dimensional structure of *E. coli* 16S ribosomal RNA in situ in the 30S subunit. *J Mol Biol 199*:115–136.

Capel MS, Kjeldgaard M, Engelman DM, Moore PB. 1988. Positions of S2, S13, S16, S17, S19 and S21 in the 30S ribosomal subunit of *E. coli. J Mol Biol 200*:65–87.

Davies C, Ramakrishnan V, White SW. 1996. Structural evidence for specific S8-RNA and S8-protein interactions within the 30S ribosomal subunit: Ribosomal protein S8 from *Bacillus stearothermophilus* at 1.9 Å resolution. *Structure 4*:1093–1104.

Döring T, Mitchell P, Osswald M, Bochkariov D, Brimacombe R. 1994. The decoding region of 16S RNA; a cross-linking study of the ribosomal A, P and E sites using tRNA derivatized at position 32 in the anticodon loop. *EMBO J 13*:2677–2685.

Dragon F, Brakier-Gingras L. 1993. Interaction of *E. coli* ribosomal protein S7 with 16S rRNA. *Nucleic Acids Res 21*:1199–1203.

Dragon F, Payant C, Brakier-Gingras L. 1994. Mutational and structural analysis of the RNA binding site for *E. coli* ribosomal protein S7. *J Mol Biol 244*:74–85.

Frank J, Zhu J, Penczek P, Li Y, Srivastava S, Verschoor A, Radermacher M, Grassucci R, Lata RK, Agrawal RK. 1995. A model of protein synthesis based on cryo-electron microscopy of the *E. coli* ribosome. *Nature 376*:441–444.

Golden BL, Hoffmann D, Ramakrishnan V, White SW. 1993. Ribosomal protein S17; characterization of the three-dimensional structure by ^{1}H and ^{15}N NMR. *Biochemistry 32*:12812–12820.

Hosaka H, Nakagawa A, Tanaka I, Harada N, Sano K, Kimura M, Yao M, Wakatsuki S. 1997. Ribosomal protein S7: A new RNA-binding motif with structural similarities to a DNA architectural factor. *Structure 5*:1199–1208.

Kimura M. 1991. The nucleotide sequence of *Bacillus stearothermophilus* ribosomal protein S12 and S7 genes; comparison with the str operon of *E. coli. Agric Biol Chem 55*:207–213.

Lake JA. 1982. Ribosomal subunit orientation determined in the monomeric ribosome by single and by double-labeling immune electron microscopy. *J Mol Biol 161*:89–106.

Lindahl M, Svensson A, Liljas A, Sedelnikova SE, Eliseikina A, Fomenkova NP, Nevskaya N, Nikonov SV, Garber MB, Muranova TA, Rykonova AI, Amons R. 1994. Crystal structure of the ribosomal protein S6 from *Thermus thermophilus. EMBO J 13*:1249–1254.

Möller K, Zwieb C, Brimacombe R. 1978. Identification of the oligonucleotide and oligopeptide involved in an RNA–protein cross-link induced by UV-irradiation of *E. coli* 30S ribosomal subunits. *J Mol Biol 126*:489–506.

Mueller F, Brimacombe R. 1997a. A new model for the three-dimensional folding of *E. coli* 16S ribosomal RNA. I. Fitting the RNA to a 3D electron microscopic map at 20 Å. *J Mol Biol 271*:524–544.

Mueller F, Brimacombe R. 1997b. A new model for the three-dimensional folding of *E. coli* 16S ribosomal RNA. II. The RNA–protein interaction data. *J Mol Biol 271*:545–565.

Mueller F, Stark H, van Heel M, Rinke-Appel J, Brimacombe R. 1997. A new model for the three-dimensional folding of *E. coli* 16S ribosomal RNA. III. The topography of the functional centre. *J Mol Biol 271*:566–587.

Nicholls A, Sharp K, Honig B. 1991. Protein folding and association; insights from the interfacial and thermodynamic properties of hydrocarbons. *Proteins Struct Funct Genet 11*:281–296.

Nissen P, Kjeldgaard M, Thirup S, Polekhina G, Reshetnikova L, Clark BFC, Nyborg J. 1995. Crystal structure of the ternary complex of Phe-tRNA^{Phe}, Ef-Tu and a GTP analog. *Science 270*: 1464–1472.

Nowotny V, Nierhaus KH. 1988. Assembly of the 30S subunit from *E. coli* ribosomes occurs via two assembly domains which are initiated by S4 and S7. *Biochemistry 27*:7051–7055.

Powers T, Noller HF. 1995. Hydroxyl radical footprinting of ribosomal proteins on 16S rRNA. *RNA 1*:194–209.

Ramakrishnan V, White SW. 1992. The structure of ribosomal protein S5 reveals sites of interaction with 16S rRNA. *Nature 358*:768–771.

Reinbolt J, Tritsch D, Wittmann-Liebold B. 1978. The primary structure of ribosomal protein S7 from *E. coli* strains K and B. *FEBS Lett 91*:297–301.

Rinke-Appel J, Jünke N, Brimacombe R, Lavrik I, Dokudovskaya S, Dontsova O, Bogdanov A. 1994. Contacts between 16S ribosomal RNA and mRNA, within the spacer region separating the AUG initiator codon and the Shine–Dalgarno sequence; a site-directed cross-linking study. *Nucleic Acids Res 22*:3018–3025.

Stade K, Rinke-Appel J, Brimacombe R. 1989. Site-directed cross-linking of mRNA analogues to the *E. coli* ribosome; identification of 30S ribosomal components that can be cross-linked to the mRNA at various points 5′ with respect to the decoding site. *Nucleic Acids Res 17*:9889–9908.

Stark H, Mueller F, Orlova EV, Schatz M, Dube P, Erdemir T, Zemlin F, Brimacombe R, van Heel M. 1995. The 70S *E. coli* ribosome at 23 Å resolution; fitting the ribosomal RNA. *Structure 3*:815–821.

Stark H, Orlova EV, Rinke-Appel J, Jünke N, Mueller F, Rodnina M, Wintermeyer W, Brimacombe R, van Heel M. 1997a. Arrangement of tRNAs in pre- and posttranslocational ribosomes revealed by electron cryomicroscopy. *Cell 88*:19–28.

Stark H, Rodnina MV, Rinke-Appel J, Brimacombe R, Wintermeyer W, van Heel M. 1997b. Visualization of elongation factor Tu on the *E. coli* ribosome. *Nature 389*:403–406.

Stern S, Weiser B, Noller HF. 1988. Model for the three-dimensional folding of 16S ribosomal RNA. *J Mol Biol 204*:447–481.

Stöffler G, Stöffler-Meilicke M. 1984. Immuno electron microscopy of ribosomes. *Annu Rev Biophys Bioeng 13*:303–330.

Urlaub H, Kruft V, Bischof O, Müller EC, Wittmann-Liebold B. 1995. Protein–rRNA binding features and their structural and functional implications in ribosomes as determined by cross-linking studies. *EMBO J 14*:4578–4588.

Urlaub H, Thiede B, Müller EC, Brimacombe R, Wittmann-Liebold B. 1997. Identification and sequence analysis of contact sites between ribosomal proteins and rRNA in *E. coli* 30S subunits by a new approach using matrix-assisted laser desorption/ionization-mass spectrometry combined with N-terminal microsequencing. *J Biol Chem 272*:14547–14555.

Wimberly BT, White SW, Ramakrishnan V. 1997. The structure of ribosomal protein S7 at 1.9 Å reveals a β-hairpin motif that binds double-stranded nucleic acids. *Structure 5*:1187–1198.

Wower J, Sylvers LA, Rosen KV, Hixson SS, Zimmermann RA. 1993. A model of the tRNA binding sites on the *E. coli* ribosome. In: Nierhaus KH, Franceschi F, Subramanian AR, Erdmann VA, Wittmann-Liebold B, eds. *The translational apparatus; Structure, function, regulation, evolution*. New York: Plenum press. pp 455–464.

Zwieb C, Brimacombe R. 1979. RNA–protein cross-linking in *E. coli* ribosomal subunits; precise localization of the nucleotide in 16S RNA which is coupled to protein S7 by UV-irradiation. *Nucleic Acids Res 6*:1775–1790.